HHS Public Access

Author manuscript

Nanophotonics. Author manuscript; available in PMC 2019 June 11.

Published in final edited form as:

Nanophotonics. 2019 January ; 8(1): 99–116. doi:10.1515/nanoph-2018-0134.

Intraoperative biophotonic imaging systems for image-guided interventions

Salar Sajedi, **Hamid Sabet**[*], and **Hak Soo Choi**[*]

Gordon Center for Medical Imaging, Department of Radiology, Massachusetts General Hospital and Harvard Medical School, Boston, MA 02114, USA

Abstract

Biophotonic imaging has revolutionized the operation room by providing surgeons intraoperative image-guidance to diagnose tumors more efficiently and to resect tumors with real-time image navigation. Among many medical imaging modalities, near-infrared (NIR) light is ideal for image-guided surgery because it penetrates relatively deeply into living tissue, while nuclear imaging provides quantitative and unlimited depth information. It is therefore ideal to develop an integrated imaging system by combining NIR fluorescence and gamma-positron imaging to provide surgeons with highly sensitive and quantitative detection of diseases, such as cancer, in real-time without changing the look of the surgical field. The focus of this review is to provide recent progress in intraoperative biophotonic imaging systems, NIR fluorescence imaging and intraoperative nuclear imaging devices, and their future perspectives for image-guided interventions.

Keywords

intraoperative imaging; biophotonic imaging; multimodal imaging; gamma-NIR imaging; image-guided surgery

1 Introduction

Biophotonic imaging utilizes various optical imaging technologies to detect biological objects and diseases with light that plays an integral role in the biomedical research field [1]. From the first use of optical imaging in the operation room (OR), many instruments have been developed to guide surgeons in real-time diagnosis and image-guided tumor resection [2]. Surgeons predominantly rely on their visual and tactile ability to distinguish healthy and unhealthy tissues during surgery, and it is therefore highly desirable to add real-time surgical guidance to the target tissue with visual characteristic and contrast. Different physical properties of targeted tissues can be exploited to provide contrast for the surgeon that the naked eye cannot easily distinguish. Since the use of extra devices comes with ergonomic limitations, the produced sensitivity and specificity of contrast should be good enough to convince the surgeon to use it [3].

[*]**Corresponding authors: Hamid Sabet and Hak Soo Choi,** Gordon Center for Medical Imaging, Department of Radiology, Massachusetts General Hospital and Harvard Medical School, Boston, MA 02114, USA, hsabet@mgh.harvard.edu (H. Sabet); hchoi12@mgh.harvard.edu (H.S. Choi).

To offer surgeons real-time quantitative information in the OR, many efforts have been made by translating spectral imaging modalities from existing preoperative nuclear imaging techniques, such as computed tomography (CT), single photon emission CT (SPECT), or positron emission tomography (PET) [4–7]. However, it has been a challenge to provide real-time feedback to surgeons during operation procedures due to 3D image-rendering processing [8]. On the other hand, near-infrared (NIR) fluorescence light penetrates relatively deeply into living tissue, thus providing the NIR window (a.k.a. Optical Window or Therapeutic Window; 650–1350 nm) in biological tissue [9]. Tissue absorption, scattering, and autofluorescence are minimum in the NIR window, thus enabling real-time image-guided surgery [10, 11]. While nuclear imaging provides quantitative depth information due to high gamma penetration, optical fluorescence imaging provides relatively high temporal and spatial resolution [12–15]. It is therefore ideal to develop an integrated imaging system by combining NIR fluorescence and gamma-positron imaging to provide surgeons with highly sensitive and quantitative detection of diseases, such as cancer, in real-time without changing the look of the surgical field. There are indeed many clinical reports supporting the benefits of using dual-modal gamma-NIR imaging in the OR [16–20]. Such a hybrid modality requires the use of radiofluorescence imaging tracers to target specific tissues and/or organs. Therefore, it is also equally important to design a hybrid contrast agent using the same fluorophore scaffold without adding additional chelators for radiotracer binding. Currently, however, a simple mixture of ^{99m}Tc nanocolloid-indocyanine green (ICG) is the most frequently used dual-modal tracer in the clinic [21, 22].

Other than gamma and fluorescence imaging, many other single or combined (also called “dual-modal” or “hybrid”) imaging modalities have been investigated or used in OR, such as Cerenkov luminescence imaging [23, 24], optical coherence tomography [25, 26], optoacoustic imaging [27], fluorescence and photoacoustic imaging [28], Raman spectroscopy [29], thermography imaging [30], chemiluminescence imaging [31], confocal endomicroscopy [32], and fluorescence lifetime imaging [33]. More efforts have recently been made to provide clinical and preclinical use of these hybrid intraoperative imaging systems in the OR. The most recent examples of intraoperative nuclear-NIR imaging systems are covered comprehensively by Bugby et al. [34]. Therefore, the focus of this review is to provide an overview of intraoperative nuclear-NIR imaging systems and future perspectives on real-time image-guided surgery.

2 NIR fluorescence imaging

Optical fluorescence imaging can guide human eyes beyond the natural limitation in terms of spatial resolution with the assistance of endogenous and/or exogeneous contrast agents [11]. Fluorescence imaging can obtain detailed molecular structures with high spatial resolution in real time. However, the ability to visualize over the surface of tissue (i.e. deep tissue imaging) and the ability to quantify molecular structures in living organisms are two of the most challenging features that fluorescence imaging aims to achieve. Ultraviolet (UV; 200–400 nm) and visible wavelengths (400–650 nm) have been used for disinfection and *in vitro* molecular diagnosis (e.g. fluorescence microscopy) but are limited for real-time *in vivo* imaging due to superficial tissue penetration of light and autofluorescence from endogenous fluorophores in the body. Therefore, the NIR window (650–1350 nm) is more attractive for

biophotonic imaging due to low tissue absorption, low tissue scattering, and low autofluorescence, which together allow imaging devices to see behind the tissue surface [11]. In addition, as the fluorescence imaging depends on both the excitation light source and collection of emission lights, the tissue penetration in the NIR window is desirable (Figure 1).

2.1 Food and Drug Administration-approved NIR fluorescent imaging systems

NIR fluorescence imaging is useful for real-time navigation of target tissues and their image-guided surgery when combined with corresponding tissue-specific fluorophores [10]. Thus, the clinical utility of NIR fluorescence imaging is closely related to the development of nontoxic imaging probes. Since the first approval for human use by the US Food and Drug Administration (FDA) in 1959, ICG (807/822 excitation/emission wavelengths) remains the only available NIR fluorescent small molecule despite intrinsic limitations such as high background uptake, intestinal contaminations, and a short blood half-life [14, 35]. Although methylene blue (MB; 665/686 excitation/emission wavelengths) has been used in the clinic historically [36], it suffers from poor optical properties for imaging purpose (Figure 2), including extremely quick excretion and rapid inactivation due to the enzymatic reduction by thiazine reductase [37], which together limits its FDA approval [38, 39]. Another combinatorial fluorophore that has been used in the clinic is 5-aminolevulinic acid (5-ALA) and protoporphyrin IX (PpIX) for imaging malignant glioma cells. 5-ALA is nonfluorescent but is a natural biochemical precursor of hemoglobin that evokes accumulation fluorescent PpIX (405 & 635/635 & 705 nm excitation/emission wavelengths) in cancerous tissues [40, 41]. Since the FDA approval in 2017, 5-ALA/PpIX has been used for tumor delineation and photodynamic therapy in the brain. Although its clinical outcomes have been promising, there are some limitations of using 5-ALA/PpIX in the clinic: (1) it is most likely to have positive porphyrin accumulation in only grade III and IV gliomas, (2) the tumor delineation is poor due to the surrounding vague fluorescence in the visible range, and (3) patients suffer from long-lasting (2–4 weeks) skin sensitivity after treatment [40–42].

Nonetheless, there is clearly an unmet clinical need to develop novel or improved fluorophores presenting high optical properties, optimal biodistribution and clearance, and minimum to no nonspecific uptake (i.e. off-target binding) for clinical use [43, 44]. While ICG and MB have frequently been used in the clinic, many polymethine and oxazine derivatives in the NIR window have been developed and used in structural visualization of anatomical features, including nerve [45], vasculature [36, 44], lymph nodes [46, 47], ureter [36, 44], bile duct [48], bone [49] and cartilage [50], and various cancers [43, 51, 52]. Due to the optical stability and tissue targetability, many efforts have also been made to translate these NIR fluorophores into the clinic. Currently, negatively charged IRDye800CW (774/789 nm excitation/emission wavelengths) and zwitterionic ZW800–1 (772/788 nm excitation/emission wavelengths) are pioneering fluorophores in clinical trials with potential in targeting tumors and diseased tissues [53].

The broad view and tactile information in open air surgery helps surgeons to detect the diseased tissue easier than in minimally invasive surgery. This fact indicates the importance of NIR fluorescence navigation in laparoscopy endoscopy, thoracoscopy, and robotic surgery

when the surgeon has only limited visual ability. This clinical need made the many research groups to integrate NIR imaging systems to the available minimally invasive surgical equipment [12–15]. Now, with the growth and popularity of minimally invasive surgeries, there are many FDA approved commercial devices available for laparoscopy, endoscopy, and robotic surgery. Figure 3 and Table 1 show a summary of commercially available open-air, laparoscopy/endoscopy, and robotic surgery fluorescence imaging systems with their significant features. The details for biophotonics will be discussed in the following sections.

2.1.1 Excitation light sources—Fluorescence is only one of the pathways that may occur after an incident photon promotes a chemical species from ground state S0 to excited S1, S2, and beyond (Figure 4). Energetic relaxation occurs through several pathways [10]. Internal conversion is shown in red in Figure 4, and corresponds to molecular movements (vibration, stretching, twisting, etc.). Another competing pathway is the process of fluorescence or the release of light of lower energy (higher wavelength) than that absorbed (energy difference is the origin of the Stokes shift). Lastly, the spin inversion from an excited singlet state to an excited triplet state can relax back to the spin paired ground state through a time-lapsed phosphorescence pathway. Building on these principles, the excitation source may be optimized such that fluorescence dominates the alternate pathways, which affords a high quantum yield of photon emission [10].

The excitation source for open-air imaging systems can be chosen according the spectral bandwidth, solid angle of output beam, light output efficiency, application-dependent regulation, cost, and lifespan [12, 15]. The fluorescence light in the open-air or microscopy surgery can be illuminated via optical fiber or directly from excitation source, but in laparoscopic/endoscopic surgery, the designated optical path should carry NIR excitation as well as white light to the field of view (FOV). For optimal fluorescence imaging, light sources should be able to illuminate the fluorophore at the center of its peak absorption wavelength through dichroic mirrors and bandpass filters [12, 15]. The most commonly used visible-NIR excitation sources are (1) filtered broadband lamps, (2) laser diodes (LDs), and (3) light-emitting diodes (LEDs). Filtered broadband lamps provide an economical option to build fluorescence imaging devices (e.g. absorption/transmission/reflectance spectroscopy and surgical microscopy) [12, 15]. High-pressure arc lamps generate an intense and broad spectrum of light from UV-vis to NIR: 200–600 nm for mercury-arc lamp and 220–750 nm for xenon lamp, while incandescent lamps (e.g. tungsten-halogen) provide wide spectral and spatial illumination from 350 to 2500 nm. This is the simplest light source and is useful for spectrometers to measure transmission and absorption. However, the low light efficiency worsens by additionally rejected photons in the emission filter to confine the output bandwidth. Thus, the produced excess heat and difficulty to focus the emission light in the open-air surgery devices toward the desired FOV make it not a suitable choice for an advanced surgical imaging system [12, 15]. Recently, supercontinuum light source has been used for femtosecond lasers and photonic crystal fibers to illuminate tunable ultrabroadband light from visible to NIR based on the propagation of high-power pulse [55]. Optical fibers deliver such high-spatial-coherence light through bandpass filters, of which cost is higher than other lamps. Supercontinuum generates a smooth spectrum and is mostly used for optical coherence tomography and not a reasonable choice for real-time imaging device.

LD has the highest spatial and spectral confinement and thus is commonly used for fluorescence and Raman spectroscopy [12, 15]. Since the spectral bandwidth of LD is narrow, for intraoperative imaging, a beam expander is specially required to broaden the illumination area for the desired FOV coupled with a wide range of dichroic mirrors and emission filters [12, 15]. Due to coherence, a blurring mechanism may also be required to overcome the speckle effect of laser sources, which can be compensated either by rotating a diffuser or vibrating a fiber [14]. Owing to the concerns on heat generation, over current and safety, the out power and temperature of high-power LDs should be carefully controlled and maintained. High temperature also reduces the lifetime of LDs drastically. Additionally, the maximal permitted exposure according to the laser class, can trigger safety concerns, and in this case, personal protective equipment such as laser goggles should be equipped in the OR to protect eyes [12, 14]. Fluoptics Fluobeam, Iridium VisionSense, and Novadaq imaging systems are currently equipped with LDs to excite exogenous fluorophores.

LED light sources are vastly used in industry and research, which lower the cost of intraoperative imaging systems in comparison to LD-based illumination [56, 57]. LEDs have broader bandwidth and illumination and usually provide lower power excitation light compared to LDs [12, 15, 58]. An array of LED illuminators is typically used to produce homogenous light over the desired FOV and excitation and emission filters confine output photon wavelength to the optical window of fluorophore(s). LED light sources with confined spectrum in the visible band are mostly used; however, a failure of such filtering increases the leakage from excitation to emission as well as the background noise level [57]. Additionally, due to the recent advancement in developing high-power LEDs, many optical imaging devices utilize LED light sources, including Hamamatsu PDE and Quest Medical Spectrum (former Artemis). However, some challenges still remain, such as light leaking due to the small Stokes shift of fluorophores, temperature control, and difficulty in assembling large and dense arrays [57].

2.1.2 Collection optical components and emission filters—The optical path from emitting fluorophores to image sensors determines the working distance (WD), FOV, image contrast, and general image quality [13]. While the details are beyond the scope of this review, here, we briefly describe each component for real-time fluorescence imaging. First, WD is of great importance given that the camera should not interfere with operation procedures, while providing an optimum FOV for intraoperative navigation [59]. With large FOV options available on many systems (e.g. Fluobeam), it is important to consider image uniformity and quality across the field at the maximum WD. While the appropriate WD depends heavily on the application, typically 20–60 cm WD with a FOV size as large as 20 × 14 cm^2 is reported for open-air surgery in the clinic (Table 1). Fluorescence images should stay in focus using an autofocus function at the maximum WD, allowing surgeons more workspace during surgical procedures. Next, the aperture of the collecting lens controls the amount of light photon collection, where a larger light collection translates to a brighter image, which in turn affects the camera exposure time and speed that might be important for near real-time imaging. Additionally, lens f# is directly related with the focal length and inversely with the pupil diameter; therefore, a large focal length leads to a small but magnified FOV with limited light collection. Finally, filter design directly depends on the

targeted fluorophores and have a critical effect on image contrast. The parameters to choose right filters are the Stokes shift of fluorophores with the spectral overlap among the excitation and emission lights as well as ambient lighting spectrum. In different applications, bandpass and notch filters can be used to remove spectral tails and overlaps.

2.1.3 Imaging sensor—Charge-coupled device (CCD)-based cameras are commonly used in fluorescence imaging devices. CCD cameras have high resolution, and the image noise can be reduced in the presence of cooling system [14]. Although they suffer from low quantum efficiency in the NIR wavelength range and slow read-out time (<30 Hz), most real-time imagers are equipped with CCD cameras because of cost efficiency (Table 1). Electron multiplied-CCDs (EMCCDs) and intensified-CCDs (ICCDs) can provide improved sensitivities with higher gains, while suffering from high background noise [12]. On the other hand, scientific complementary metal-oxide-semiconductor cameras deliver fast readout speeds, high bit depth, high sensitivity, high quantum efficiency, wide dynamic range, and low read-out noise without the addition of multiplicative noise associated with EMCCDs [59]. However, the cost is still expensive compared to standard CCD cameras, which could be improved in the near future. Currently, Perkin Elmer Solaris is the only one adapting this most advanced technology in the imager [59].

2.1.4 Image overlay—The graphical user interface of most handheld imagers, such as Fluoptics Fluobeam, Hamamatsu PDE Neo, and Novadaq SPY, provides a single channel fluorescence video/image display. Although such simple intraoperative image display would be sufficient in the OR, real-time overlay of color images with the fluorescence signals can provide significantly improved procedures for surgeons to find the target tissue without looking back at the color video [60, 61]. This is also important for spectral multiplexing of optical photons when two or more different imaging fluorophores are used at the same time to delineate the target tissue and vital tissues, such as vasculature, nerve, and endocrine glands [61]. For simultaneous overlaying of color video and fluorescence images, most imagers are equipped with beam splitters and a combination of multiple cameras. Currently, many efforts have been made to separate visible and NIR fluorescence wavelengths within the camera itself using prism coatings and multiple CCD or complementary metal-oxide-semiconductor (CMOS) sensors, which will be available clinically in the near future. It should be noted that in the case of two or more channels are being displayed, a poor color map selection for the image overlay may lead to misrepresentation of reality and misinterpretation; however, good color map selection can highlight clinically salient regions. Image overlay for fluorescence imaging is reviewed in Ref. [60].

2.1.5 Ambient light—IEC standard #60601 for the OR illumination dictates that minimum central luminance of the surgical field must be at least 40,000 lux at the typical WD [58]. Further, it declares that the color temperature must be between 3000 and 6700 K with a color rendering index ≥85. This color pattern is required to avoid the surgical field being preferentially “tinged” with one or more visible colors [14]. Most filtered broadband and LED white light sources can be used for providing white light to the surgical field. Since the illumination sources in the OR may have significant fraction in the NIR range, special care is required to avoid noise and background signals polluted by the ambient light. In this

regard, LED light sources with confined spectrum in the visible band are mostly used. Additionally, due to the recent advancement in developing high-power LEDs, many optical imaging devices utilize LED light sources, including Hamamatsu PDE and Quest Medical Spectrum (former Artemis). However, some challenges still remain, such as light leaking due to the small Stokes shift of fluorophores, temperature control, and difficulty in assembling large and dense arrays [57].

2.2 Optical fluorescence imaging: pros and cons

Optical fluorescence imaging provides simple, cost-efficient, and contact-free open-air image-guidance during surgical operation, where fluorophores are excited by an appropriate light source and the emitted photons are detected by CCD or CMOS cameras. Fluorescence imaging is highly compatible with the intraoperative setting, as it enables real-time imaging and offers superior sensitivity compared to preoperative scanning or visual inspection and palpation during surgical procedures [11].

The NIR window is usually preferred for *in vivo* imaging because of lower autofluorescence, deeper tissue penetration, and reduced light absorption and scattering [11]. Wearable display goggles and novel projection strategies have been proposed to obviate standard monitor displays that require the surgeon to divert his/her gaze from the operative field [62]. However, scattering of excitation light by subcellular organelles and other microscopic tissue constituents greatly limits its penetration into deep-seated targets up to 5 mm in depth, which degrades spatial resolution [14]. Thus, due to scattering and absorption in both excitation and emission path, in addition to finite quantum yield of fluorophores, only one-millionth to one-billionth of photons can be detected using the current reflectance-based imaging systems [63]. This low detection rate also limits the quantification of fluorophore concentrations in the tissue. This uncertainty in the scattering, absorption, and quantum yield leads to only qualitative information from NIR fluorescence image [63]. Consequently, many efforts have been made to compensate the attenuation effect in the NIR imaging and improve image contrast and target detection [64–66]. It is indeed feasible to obtain the quantitative assessment of fluorophore uptake in tissues with complete modeling of attenuation and quantum yield using intraoperative fluorescence microscopy [64]. Additionally, in perfusion studies, relative measurements of tissues over time could provide quantitative kinetic information without requiring the attenuation models [65, 66]. However, the quantitative feature of fluorescence imaging is still far from the final clinical application.

3 Nuclear imaging and navigation

Radiation medical imaging using ionizing particles has revolutionized the surgical interventions because gammaray and x-ray penetration into tissue enables physicians to observe tumors deep within tissue without surgical intervention, before, during, and after operation [67]. Anatomical X-ray and CT, along with functional and behavioral imaging using SPECT and PET, are powerful tools in patient screening, tumor staging and restaging and therapeutic procedures. While nuclear medicine (e.g. PET and SPECT/gamma-camera) and X-ray/CT imaging modalities account for two out of four key modalities (the other two are ultrasound and magnetic resonance imaging) in all radiology departments across

hospitals and medical centers, they typically fail to detect small-size tumors or tumorous lymph nodes [68]. This is mainly due to the limited sensitivity and resolution characteristics of PET and SPECT as well as error factors such as the partial volume effect of the current nuclear imaging modalities. The primary reason is simply the geometry of these systems – the location of their detectors is many centimeters away from the lesion of interest and poor sensitivity of these systems that can pick only about 1% of all gamma-rays originating within human body. Reviewing literature indicates that whole-body PET with ~4–5 mm spatial resolution can reliably detect lymph nodes larger than 0.5 cm, and they have very low sensitivity to detect nodes smaller than 5 mm [68]. The inability of these conventional noninvasive modalities to detect small objects, has led to the development of intraoperative devices that are used in closer distance to the tissue of interest, resulting in larger detector solid angle and, thus, higher detection sensitivity and spatial resolution [67–69]. In other words, the geometry of detection is in favor of these intraoperative probes compared with the standard nuclear medicine modalities.

For intraoperative localization of gamma emitting tracers in real-time, a handheld gamma radio-detection probe, first conceived in 1949, is generally used in conjunction with radiotracers that are injected directly into or next to suspected lesions prior to surgery [69]. Gamma and beta (positron) probes are powerful tools in sentinel lymph node (SLN) localization and biopsy and have become the standard of care in which surgeons use audio, numeric, and/or visual guidance (using flashing arrows), instead of using image navigation [70]. Recently, the use of intraoperative imaging (gamma and/or beta) cameras that can provide an image of radiotracer distribution in the region of interest (ROI) has been on the rise. Conventional gamma cameras can provide size and shape information about the tumor, SLN, or other targeted tissues [69]. Throughout the years of development, however, a clear line to differentiate intraoperative probes from conventional cameras has somewhat diminished especially for multimodal and multifunctional devices (see Section 3.3). In the following sections, we provide an overview of gamma- and beta-based intraoperative devices, with a special focus on gamma-ray imaging cameras.

3.1 Intraoperative gamma imaging

Intraoperative gamma probes consist of both imaging and nonimaging probes that are based on the detection of gamma-rays emitted from radiotracers distributed inside the body. Most gamma probes provide either audio or visual guidance (e.g. arrow) to navigate surgeons to the tumor site; however, it can be more beneficial if gamma probes can provide images of the radiotracer distribution within its FOV, while using the same detection concept. Figure 5 shows gamma imaging commonly used in hand-held or portable devices. In the 1990s, the intraoperative gamma camera became a complementary detection method for SLN detection in breast cancer surgery [72]. In this context, these devices consist of a small handheld camera for use during surgery, while larger FOV devices are attached to an articulating arm for easy and stable positioning (Figures 5 and 6). These systems are nonetheless fully portable with small footprint for easy accommodation in a typical OR.

Intraoperative gamma cameras have been introduced to SLN detection for various cancer types, including breast cancer [77–79], head and neck [80], laryngeal [81], oral [82],

gastrointestinal [83], paraaortic SLN [7], and testicular cancer [84]. Gamma cameras also allow SLN detection using iodine seed localization with laparoscopy surgery [85]. Other than SLN detection, portable gamma cameras have been reportedly used in occult lesion localization [86], tumor-specific targeting [87], and parathyroidectomy [88, 89]. Although the use of nonimaging gamma probes in the SLN surgery is a standard tool, providing images by using handheld gamma cameras has additional advantages for better visualizing the primary tumor, SLN, and auxiliary nodes. Vidal-Sicart et al. demonstrated the added value of intraoperative gamma imaging in SLN localization among 20 patients selected with respect to preoperative imaging data, whose SLN were found to be difficult to detect [90]. In patients with breast cancer, malignant melanoma, and gynecologic malignancy, the surgeon could find all SLNs in 15 out of 20 patients with utilization of a conventional gamma probe. Further, the portable gamma camera enabled detection of SLNs in 19 of 20 patients, leading to successful resection. In one patient, a harvested SLN was metastatic, which could be missed without using the camera [90].

In breast cancer, the combination of gamma probe and blue dye is the standard procedure for SLN biopsy. A meta-analysis of 70 published research reports on breast cancer SLN biopsy shows an overall sensitivity of 90% and false-negative rate of 8.4% [91]. Where the preoperative lymphoscintigraphy revealed 70–85% detection rate, the use of intraoperative gamma imaging probe (camera) found 98% of SLNs with 7% of false-negative detection (Figure 7) [94]. When using the gamma probe to find SLN near the injection site, high activity may block visibility of nodes with small activity compared with the primary tumor, the so-called the “shine-through” effect [92]. However, due to the superior resolution and overall performance, the use of gamma probe or camera facilitated the detection of low-activity nodes near the high-activity region. The spatial intrinsic resolution of some of the most used imaging gamma probes in the OR is presented in Table 2, while the system spatial resolution is variable with the object distance from the collimator.

The length of imaging time is a function of injected activity, time between injection and image acquisition, tissue thickness between nodes and surface of detectors, and sensitivity of the imaging gamma camera/probe. Reported acquisition times in various studies ranged from 10 to 180 s [82]. Although the portable gamma camera provides additional values for SLN detection, procedures take more time than using a gamma probe and optionally blue dyes because the count statistics increase with image pixel size (needed for high resolution image) [103]. Here, we provide brief descriptions on the most important components of gamma probes, namely detector and collimator, and potential add-ons such as optical image overlay.

3.1.1 Gamma detectors—There are two main schemes for gamma-ray detection: (1) Direct conversion, where the semiconductor detector directly converts the incident radiation to electric signal, and (b) indirect conversion, which involves with using scintillation crystal(s) to convert the incident gamma-ray to optical photons and then a photodetector or array of photodetectors to convert the optical photons to electric signal [76]. Each detector scheme has its own pros and cons, and both types have been widely used in imaging and nonimaging intraoperative gamma probes. Typically, the end application requirements drive the choice of direct or indirect conversion detector. For example, if high energy resolution or

small overall detector size is demanded, direct conversion detectors such as CdTe or cadmium zinc telluride semiconductors are more suitable [104]. On the other hand, if the application requires low cost and large imaging area, scintillator-based detectors have the upper hand. Prior to emergence of novel photodetectors such as solid-state or silicon photomultipliers (SiPMs), conventional photomultipliers (PMTs) were the obvious choice compared with bulky CCD cameras that required cooling. PMTs have better noise performance compared to SiPMs, resulting in better overall energy resolution, especially at low gamma-ray energies, but they are bulky and require high bias voltage, typically ~1000 V. SiPMs require bias voltages below 70 V and are very compact and lightweight, which has enabled wireless intraoperative probes [105]. SiPMs are, however, more sensitive to temperature and have larger dark current or dark count leading to larger noise level [106]. With the growth of the SiPM market and presence of competitive vendors in the gamma imaging devices, the quality of SiPM technology is improving very fast, which indicates that these devices will likely replace PMTs in future gamma cameras.

3.1.2 Collimators—In imaging applications with single gamma-ray photons, there is a strong need for a collimator in front of the detector to limit the camera's FOV since gamma-rays can travel far from the emitting location (Figure 5). It is apparent that the collimators should be made up of high-Z and -density materials with a large cross-section to stop gamma-rays. Lead (Pb) and tungsten (W) are the two main materials used in collimators. Furthermore, the two most commonly used collimator types in commercial and prototype hand-held cameras are parallel-hole and pinhole collimators. The major difference between these two is their FOV and magnification factor, which affect all other camera properties as well. Similar to the infamous optical pinhole camera, the magnification changes by object distance and that itself changes system resolution and sensitivity in the pinhole collimator. This variability, in practice, gives surgeons the ability to adjust the FOV by increasing distance from the object. The downfall of adjustable magnification is that if the depth of the ROI is unknown, the actual size of the object can be misleading. However, gamma camera resolution worsens with increased distance between object and detector with both collimator types. For example, the resolution can be lower than 2 mm for the intraoperative applications when there is no distance between the camera and the object, but this value can rapidly degrade to greater than 20 mm with a 10 cm object distance [73, 92].

3.1.3 Optical image overlay—Providing optical images of the surveyed area is obviously an advantageous addition to the radiation image, resulting in improved localization of the tissue of interest. Here, we only provide a brief overview of few approaches. One approach is to use laser pointers to shine and mark the surveyed area for the surgeon, which has been exercised and reported by investigators such as Vermeeren et al. [80]. A prototype gamma-optic system was developed by Haneishi et al. [107] using dual optical cameras and image processing technique to fuse radio and optical images in the OR. A similar concept is used in [93] for a smaller FOV. Errors in the optical image coregistration were evaluated with a 5-mm accuracy for each patient. In another effort, Lees et al. [71] proposed an integrated radio-optical system where a mirror is placed right before the gamma camera's pinhole routing optical photons to a CCD camera. This geometry has

the advantage of intrinsic co-registration of nuclear-optic FOV geometry and therefore does not require additional image processing.

3.1.4 Challenges in gamma imaging—There are two main shortcomings with gamma-ray imaging probes: First, the mandatory use of a collimator placed in front of the detector substantially limits the sensitivity. This can be compensated, to some extent, by increasing the administered patient dose, which may not be the best solution as it causes excessive radiation exposure for both patients and medical staff. Secondly, the use of a collimator and shielding on the side and back makes the imaging gamma probe heavy and harder to adapt for handheld use. Therefore, the current commercial gamma imaging cameras are mounted on articulating arms for improved maneuverability to hover over patient body during surgery.

3.2 Intraoperative beta imaging

Even with the use of heavy collimators, the performance of gamma-ray probes may be severely hampered when surveying tissues with high gamma-ray background contamination. This contamination can be especially problematic when surveying areas near organs with large radiotracer uptake such as brain, heart, and bladder. Therefore, the use of gamma probes is mainly to identify SLNs in which radiotracer is injected to the tumor site that limits the tracer spread and the blind locations to the near the injection area. Due to positron-emitting nature of PET radiotracers, many groups sought methods to use the inherent low-penetrating feature of positrons to limit the probe's FOV depth to only a few mm of tissue thickness. This short range of positrons can be used for tumor localization of within 1–2 mm of the probe head, which can be useful for detecting tumor margins [108]. Positron detectors are thin and mainly made up of low-Z materials such as plastic scintillators to reduce the chance of background interaction [109]. These probes have the advantage of high particle detection efficiency and can detect very small concentrations of radiotracer [110, 111]. This, along with lower sensitivity to high gamma energies that can be handy in high background gamma activity region, makes them ideal in detecting low-activity nodes in the presence of high background activity. Monge et al. also proved that freehand positron surface imaging equipped with a navigation tool and a simple beta probe could generate 3D iso-surface images (mesh) and additional information of residual tumors during surgery [112]. Although beta imaging has superior sensitivity and resolution compared to gamma imaging, the fundamental limit of this modality remains to the limited penetration of beta radiation up to a few mm, of which attenuation also limits the ability of quantitative assessments [110]. Thus, the combination of beta imaging with NIR fluorescence is not ideal. This also should be noted that ^{18}F-FDG based radio-guided surgeries show 2- to 3-fold higher dose absorption to intra- and pre-operative personnel compared to the use of ^{99m}Tc [113]. As dictated in Table 3, the cumulative dose of surgeon for an operation is calculated 1–40 μSv for ^{99m}Tc radioisotope [114, 115] and 16–160 μSv for ^{18}F radioisotope [113, 116]. The elevated dose received by surgeons is correlated to the diverse distribution of ^{18}F-FDG in patient's body compared to locally injected ^{99m}Tc-labeled tracers as well as the higher gamma energy produced from positron annihilation (511 keV) for ^{99m}Tc (140 keV). The annual occupational exposure limit for adults is, on average, 20 mSv per year in a 5-year period (100 mSv in 5 years) [117].

3.3 Radio-guided navigation systems

The depth of object is unknown with a single gamma image projection. With acquiring multiple projections, however, the object depth can be estimated with a high accuracy. One specific example is the freehand SPECT system, a commercially available device that can generate 3D images with depth information in the OR, which has been used for intraoperative SLN biopsy [118]. The freehand SPECT uses a conventional gamma probe or camera with an additional accurate positioning system (Figure 8). The navigation system generates accurate position and orientation information for the gamma probe in respect to the patient body, using infrared markers on the gamma probe and on the patient and infrared tracker (cameras) on the stationary system [119]. Operators (surgeons) should determine a volume of interest (VOI) at the beginning of each scan and then sweep the probe in the ROI. Scanning the VOI should continue to ensure that enough data for reconstructing image are gathered from gamma probe and the final image will have acceptable quality [118]. The customized image reconstruction software based on maximum likelihood expectation maximization method provides near real-time 3D images of SLNs by accumulating data entries from the gamma probe while scanning the VOI. Although it is not the standard of care in SLN biopsy, the freehand SPECT has resulted in better surgical outcomes in many types of cancer operations instead of using only acoustic gamma probes [8, 120]. However, it requires the operator's skill to generate a high-quality image [8]. The freehand SPECT is currently the only way to provide intraoperative 3D nuclear imaging and allows integration of both gamma probe and camera to the navigation system.

4 Perspectives of nuclear-NIR intraoperative imaging

In this review, we provide a brief overview of intraoperative NIR fluorescence imaging devices and intraoperative radiation probes/cameras. Gamma rays can penetrate much deeper in tissues with low chance of scattering compared with optical photons, whose penetration is limited and have a high change of scattering. On the other hand, with NIR fluorescence imaging, one can achieve very high spatial and temporal resolution that cannot be achieved with gamma-ray imaging. The combination of these two modalities should lead to improved tumor removal and metastatic SLN identification. In many clinical trials, the combination of blue dye and radiotracers has been used for dual mapping of SLN, resulting in lower false-negative rates compared with those trials that used only single mapping technique (i.e. gamma-ray or blue dye) [17, 70]. Lower false-negative rates bode well with the American Society of Clinical Oncology guidelines that proposed surgical practices should aim for high identification rate of 85% and low false-negative rates of 5% [70]. Many clinical reports prove that the hybrid use of both modalities has added clinical values to SLN biopsy [17] in different cancers of breast [18], prostate [16, 121], vulvar [19, 20], penile [122], and melanomas [17].

To develop gamma-NIR dual-modal imaging devices, KleinJan et al. combined a fluorescence camera with either a gamma probe (Figure 9A) or a gamma camera (Figure 9B). This hybrid surgical guidance concept was demonstrated using a dual tracer of ICG and 99mTc-nanocolloid in cT1-cT3N0 penile cancer patients [123]. The combination of NIR-gamma probe provided real-time acoustic feedback during SLN mapping, and additional

image guidance from the NIR-gamma camera was highly valuable for visualization of SLNs in patients (10–30 cm WD). Additionally, van den Berg et al. integrated a nonimaging ICG probe to a conventional nonimaging gamma probe using optical fibers (Figure 9C,D) and evaluated the proposed concept in 41 cancer patients in the head and neck or urogenital area [124]. Recently, Kang et al. explored dual-modal imaging of gamma and NIR with white light in a laparoscopy setting [125]. The miniaturized pinhole collimator was equipped with NIR illumination and imaging fibers to transfer light to the proximal part, where a cooled CCD camera captures NIR and gamma images simultaneously. Augmented reality utilizing preoperative SPECT/CT images and intraoperative freehand SPECT as discussed in Section 3.3 can also provide quantitative detection of SLNs in combination with NIR fluorescence imaging [126].

Along with the instrumentation, many efforts have been made to develop dual-modal imaging agents for visualizing metastatic tumors and SLNs. ^{99m}Tc-nanocolloid is the basic radiotracer for radio-guided surgery, which is mostly accompanied by blue dyes or ICG for better visual feedback of finding drainage SLNs [17, 21, 22]. Brouwer et al. evaluated the use of a nanocolloid labeled with ICG and ^{99m}Tc to find SLN in head and neck surgery [17]. In the surgical procedure, an intraoperative gamma camera assisted the surgeons to find incision locations and NIR imaging visualized SLNs through the operation. Using both modalities, all preoperatively detected nodes were found during surgery. Additionally, the use of dual-labeled nanocolloid instead of traditional ^{99m}Tc-nanocolloid alone increased SLN detection rates to 85.7% and reduced the false-negative rates to 7% [21]. Since ICG is, however, nonspecific to tumoral uptake, tumor-specific dual gamma-NIR tracers have recently been designed and evaluated. One of the key design considerations is the avoidance of nonspecific uptake in the major organs and background tissue, thus increasing signal-to-background ratio [10, 11]. Vera and colleagues conjugated NIR fluorescent Cy7 to ^{99m}Tc-labeled tilmanocept and tested the hybrid tracer for SLN mapping [127] and tumor targeting in the xenograft mice of 4T1 mouse mammary and melanoma tumors [128]. Additional trials have also been performed to introduce gamma-NIR tracers on various antibodies [129], peptides [130], lipopolysaccharides [131], and short RNA sequences [132] for targeting tumors and SLNs. However, the main challenge in developing hybrid imaging tracers is on the specific tumor targeting with minimum nonspecific (i.e. off-target binding) uptake [22, 133]. Unfortunately, only a small number of radio-optical tracers have been used in the clinic, and more efforts need to be made to translate preclinical multimodal tracers to the clinic (reviewed in [25]). This is the key for future clinical translation of this hybrid imaging for tumor targeting and image-guided resection.

The use of dual-modal radio-optical tracers in conjunction with real-time coregistered images from NIR and gamma camera will be the future step in intraoperative image-guided interventions. Therefore, we believe that intraoperative imaging devices need to be evolved to combine (1) NIR fluorescence imaging for high spatial and temporal resolution, (2) gamma-ray imaging for high sensitivity with depth information, and (3) PET-like geometry for quantitative imaging.

Acknowledgments:

We thank Ivey Choi for manuscript editing. This study was supported by the US NIH/NIBIB grants #R01EB022230, #R21EB023391, and #R21EB020162. The contents of this paper are solely the responsibility of the authors and do not necessarily reflect the official views of the National Institutes of Health.

References

[1]. Cannell MB. Functional imaging: gaining new insight from biophotonic imaging. Clin Exp Pharmacol Physiol 2004;31:883–4. [PubMed: 15659053]

[2]. Kang H, Hu S, Cho MH, Hong SH, Choi Y, Choi HS. Theranostic nanosystems for targeted cancer therapy. Nano Today 2018;23:59–72.

[3]. Pogue BW, Wilson BC. Optical and x-ray technology synergies enabling diagnostic and therapeutic applications in medicine. J Biomed Opt 2018;23:1–17.

[4]. Cohn DE, Hall NC, Povoski SP, Seamon LG, Farrar WB, Martin EW Jr. Novel perioperative imaging with 18F-FDG PET/CT and intra-operative 18F-FDG detection using a handheld gamma probe in recurrent ovarian cancer. Gynecol Oncol 2008;110:152–7. [PubMed: 18539314]

[5]. Sarikaya I, Povoski SP, Al-Saif OH, et al. Combined use of preoperative 18F FDG-PET imaging and intraoperative gamma probe detection for accurate assessment of tumor recurrence in patients with colorectal cancer. World J Surg Oncol 2007;5:80. [PubMed: 17634125]

[6]. Olmos RA, Vidal-Sicart S, Nieweg OE. SPECT-CT and real-time intraoperative imaging: new tools for sentinel node localization and radioguided surgery? Eur J Nucl Med Mol Imaging 2009;36:1–5. [PubMed: 18931842]

[7]. Vermeeren L, Meinhardt W, Bex A, et al. Paraaortic sentinel lymph nodes: toward optimal detection and intraoperative localization using SPECT/CT and intraoperative real-time imaging. J Nucl Med 2010;51:376–82. [PubMed: 20150260]

[8]. Bluemel C, Schnelzer A, Okur A, et al. Freehand SPECT for image-guided sentinel lymph node biopsy in breast cancer. Eur J Nucl Med Mol Imaging 2013;40:1656–61. [PubMed: 23754763]

[9]. Smith AM, Mancini MC, Nie S. Bioimaging: second window for in vivo imaging. Nat Nanotechnol 2009;4:710–1. [PubMed: 19898521]

[10]. Owens EA, Henary M, El Fakhri G, Choi HS. Tissue-specific near-infrared fluorescence imaging. Acc Chem Res 2016;49:1731–40. [PubMed: 27564418]

[11]. Owens EA, Lee S, Choi J, Henary M, Choi HS. NIR fluorescent small molecules for intraoperative imaging. Wiley Interdiscip Rev Nanomed Nanobiotechnol 2015;7:828–38. [PubMed: 25645081]

[12]. DSouza AV, Lin H, Henderson ER, Samkoe KS, Pogue BW. Review of fluorescence guided surgery systems: identification of key performance capabilities beyond indocyanine green imaging. J Biomed Opt 2016;21:080901.

[13]. Chi C, Du Y, Ye J, et al. Intraoperative imaging-guided cancer surgery: from current fluorescence molecular imaging methods to future multi-modality imaging technology. Theranostics 2014;4:1072–84. [PubMed: 25250092]

[14]. Gioux S, Choi HS, Frangioni JV. Image-guided surgery using invisible near-infrared light: fundamentals of clinical translation. Mol Imaging 2010;9:237–55. [PubMed: 20868625]

[15]. Yang AW, Cho SU, Jeong MY, Choi HS. NIR Fluorescence imaging systems with optical packaging technology. J Microelectron Packag Soc 2014;21:25–31.

[16]. van der Poel HG, Buckle T, Brouwer OR, Olmos RAV, van Leeuwen FW. Intraoperative laparoscopic fluorescence guidance to the sentinel lymph node in prostate cancer patients: clinical proof of concept of an integrated functional imaging approach using a multimodal tracer. Eur Urol 2011;60:826–33. [PubMed: 21458154]

[17]. Brouwer OR, Klop WMC, Buckle T, et al. Feasibility of sentinel node biopsy in head and neck melanoma using a hybrid radio-active and fluorescent tracer. Ann Surg Oncol 2012;19:1988–94. [PubMed: 22207047]

[18]. Schaafsma BE, Verbeek FP, Rietbergen DD, et al. Clinical trial of combined radio-and fluorescence-guided sentinel lymph node biopsy in breast cancer. Br J Surg 2013;100:1037–44. [PubMed: 23696463]

[19]. Mathéron H, Van Den Berg N, Brouwer O, et al. Multimodal surgical guidance towards the sentinel node in vulvar cancer. Gynecol Oncol 2013;131:720–5. [PubMed: 24051219]

[20]. Verbeek FP, Tummers QR, Rietbergen DD, et al. Sentinel lymph node biopsy in vulvar cancer using combined radioactive and fluorescence guidance. Int J Gynecol Cancer 2015;25:1086–93. [PubMed: 25768079]

[21]. KleinJan GH, Bunschoten A, van den Berg NS, et al. Fluorescence guided surgery and tracer-dose, fact or fiction? Eur J Nucl Med Mol Imaging 2016;43:1857–67. [PubMed: 27020580]

[22]. Zhao J, Chen J, Ma S, et al. Recent developments in multimodality fluorescence imaging probes. Acta Pharmaceutica Sinica B 2018;8:320–38. [PubMed: 29881672]

[23]. Grootendorst M, Cariati M, Kothari A, Tuch D, Purushotham A. Cerenkov luminescence imaging (CLI) for image-guided cancer surgery. Clin Transl Imaging 2016;4:353–66. [PubMed: 27738626]

[24]. Grootendorst MR, Cariati M, Pinder S, et al. Intraoperative assessment of tumor resection margins in breast-conserving surgery using 18F-FDG Cerenkov luminescence imaging: a first-in-human feasibility study. J Nucl Med 2017;58:891–8. [PubMed: 27932562]

[25]. Nolan RM, Adie SG, Marjanovic M, et al. Intraoperative optical coherence tomography for assessing human lymph nodes for metastatic cancer. BMC cancer 2016;16:144. [PubMed: 26907742]

[26]. Ehlers J Intraoperative optical coherence tomography: past, present, and future. Eye 2016;30:193–201. [PubMed: 26681147]

[27]. Dima A, Gateau J, Claussen J, Wilhelm D, Ntziachristos V. Optoacoustic imaging of blood perfusion: techniques for intraoperative tissue viability assessment. J Biophotonics 2013;6:485–92. [PubMed: 23494993]

[28]. Tummers WS, Miller SE, Teraphongphom NT, et al. Intraoperative pancreatic cancer detection using tumor-specific multimodality molecular imaging. Ann Surg Oncol 2018;25:1880–8. [PubMed: 29667116]

[29]. Reder NP, Kang S, Glaser AK, et al. Raman-encoded molecular imaging with topically applied SERS nanoparticles for intraoperative guidance of lumpectomy. Cancer Res 2017;77:4506–16. [PubMed: 28615226]

[30]. Steiner G, Sobottka SB, Koch E, Schackert G, Kirsch M. Intraoperative imaging of cortical cerebral perfusion by time-resolved thermography and multivariate data analysis. J Biomed Opt 2011;16:016001. [PubMed: 21280907]

[31]. Büchel GE, Carney B, Shaffer TM, et al. Near-infrared Intra-operative chemiluminescence imaging. ChemMedChem 2016;11:1978–82. [PubMed: 27471800]

[32]. Lopez A, Zlatev DV, Mach KE, et al. Intraoperative optical biopsy during robotic assisted radical prostatectomy using confocal endomicroscopy. J Urol 2016;195:1110–7. [PubMed: 26626214]

[33]. Kantelhardt SR, Kalasauskas D, König K, et al. In vivo multiphoton tomography and fluorescence lifetime imaging of human brain tumor tissue. J Neurooncol 2016;127:473–82. [PubMed: 26830089]

[34]. Bugby SL, Lees J, Perkins A. Hybrid intraoperative imaging techniques in radioguided surgery: present clinical applications and future outlook. Clin Transl Imaging 2017;5:323–41. [PubMed: 28804703]

[35]. Choi HS, Frangioni JV. Nanoparticles for biomedical imaging: fundamentals of clinical translation. Mol Imaging 2010;9:291–310. [PubMed: 21084027]

[36]. Hyun H, Henary M, Gao T, et al. 700-nm zwitterionic near-infrared fluorophores for dual-channel image-guided surgery. Mol Imaging Biol 2016;18:52–61. [PubMed: 26084246]

[37]. May JM, Qu ZC, Cobb CE. Reduction and uptake of methylene blue by human erythrocytes. Am J Physiol Cell Physiol 2004;286:C1390–8. [PubMed: 14973146]

[38]. Winer JH, Choi HS, Gibbs-Strauss SL, Ashitate Y, Colson YL, Frangioni JV. Intraoperative localization of insulinoma and normal pancreas using invisible near-infrared fluorescent light. Ann Surg Oncol 2010;17:1094–100. [PubMed: 20033320]

[39]. Matsui A, Tanaka E, Choi HS, et al. Real-time, near-infrared, fluorescence-guided identification of the ureters using methylene blue. Surgery 2010;148:78–86. [PubMed: 20117811]

[40]. Chohan MO, Berger MS. 5-Aminolevulinic acid fluorescence guided surgery for recurrent high-grade gliomas. J Neurooncol 2018 (in press), 10.1007/s11060-018-2956-8.

[41]. Lakomkin N, Hadjipanayis CG. Fluorescence-guided surgery for high-grade gliomas. J Surg Oncol 2018;118:356–61. [PubMed: 30125355]

[42]. Hu S, Kang H, Baek Y, El Fakhri G, Kuang A, Choi HS. Real-Time imaging of brain tumor for image-guided surgery. Adv Healthc Mater 2018;7:e1800066. [PubMed: 29719137]

[43]. Choi HS, Gibbs SL, Lee JH, et al. Targeted zwitterionic near-infrared fluorophores for improved optical imaging. Nat Biotechnol 2013;31:148–53. [PubMed: 23292608]

[44]. Choi HS, Nasr K, Alyabyev S, et al. Synthesis and in vivo fate of zwitterionic near-infrared fluorophores. Angew Chem Int Ed Engl 2011;50:6258–63. [PubMed: 21656624]

[45]. Park MH, Hyun H, Ashitate Y, et al. Prototype nerve-specific near-infrared fluorophores. Theranostics 2014;4:823–33. [PubMed: 24955143]

[46]. Ashitate Y, Hyun H, Kim SH, et al. Simultaneous mapping of pan and sentinel lymph nodes for real-time image-guided surgery. Theranostics 2014;4:693–700. [PubMed: 24883119]

[47]. Hutteman M, Choi HS, Mieog JS, et al. Clinical translation of ex vivo sentinel lymph node mapping for colorectal cancer using invisible near-infrared fluorescence light. Ann Surg Oncol 2011;18:1006–14. [PubMed: 21080086]

[48]. Matsui A, Tanaka E, Choi HS, et al. Real-time intra-operative near-infrared fluorescence identification of the extrahepatic bile ducts using clinically available contrast agents. Surgery 2010;148:87–95. [PubMed: 20117813]

[49]. Hyun H, Wada H, Bao K, et al. Phosphonated near-infrared fluorophores for biomedical imaging of bone. Angew Chem Int Ed Engl 2014;53:10668–72. [PubMed: 25139079]

[50]. Hyun H, Owens EA, Wada H, et al. Cartilage-specific near-infrared fluorophores for biomedical imaging. Angew Chem Int Ed Engl 2015;54:8648–52. [PubMed: 26095685]

[51]. Choi HS, Liu W, Liu F, et al. Design considerations for tumour-targeted nanoparticles. Nat Nanotechnol 2010;5:42–7. [PubMed: 19893516]

[52]. Chung JE, Tan S, Gao SJ, et al. Self-assembled micellar nanocomplexes comprising green tea catechin derivatives and protein drugs for cancer therapy. Nat Nanotechnol 2014;9:907–12. [PubMed: 25282044]

[53]. Hong G, Antaris AL, Dai H. Near-infrared fluorophores for biomedical imaging. Nat Biomed Eng 2017;1:0010.

[54]. Zhu B, Sevick-Muraca EM. A review of performance of near-infrared fluorescence imaging devices used in clinical studies. Br J Radiol 2015;88:20140547. [PubMed: 25410320]

[55]. Cimalla P, Walther J, Mehner M, Cuevas M, Koch E. Simultaneous dual-band optical coherence tomography in the spectral domain for high resolution in vivo imaging. Opt Express 2009;17:19486–500. [PubMed: 19997169]

[56]. Gioux S, Kianzad V, Ciocan R, et al. A low-cost, linear, DC-35 MHz, high-power LED driver for continuous wave (CW) and fluorescence lifetime imaging (FLIM). Proc Soc Photo Opt Instrum Eng 2008;6848:684807.

[57]. Gioux S, Kianzad V, Ciocan R, Gupta S, Oketokoun R, Frangioni JV. High-power, computer-controlled, light-emitting diode-based light sources for fluorescence imaging and image-guided surgery. Mol Imaging 2009;8:156–65. [PubMed: 19723473]

[58]. Troyan SL, Kianzad V, Gibbs-Strauss SL, et al. The FLARE™ intraoperative near-infrared fluorescence imaging system: a first-in-human clinical trial in breast cancer sentinel lymph node mapping. Ann Surg Oncol 2009;16:2943–52. [PubMed: 19582506]

[59]. Behrooz A, Waterman P, Vasquez KO, et al. Multispectral open-air intraoperative fluorescence imaging. Opt Lett 2017;42:2964–7. [PubMed: 28957220]

[60]. Elliott JT, Dsouza AV, Davis SC, et al. Review of fluorescence guided surgery visualization and overlay techniques. Biomed Opt Express 2015;6:3765–82. [PubMed: 26504628]

[61]. Laios A, Volpi D, Tullis ID, et al. A prospective pilot study of detection of sentinel lymph nodes in gynaecological cancers using a novel near infrared fluorescence imaging system. BMC Res Notes 2015;8:608. [PubMed: 26502876]

[62]. Mondal SB, Gao S, Zhu N, Liang R, Gruev V, Achilefu S. Real-time fluorescence image-guided oncologic surgery. Adv Cancer Res 2014;124:171–211. [PubMed: 25287689]

[63]. Vahrmeijer AL, Hutteman M, van der Vorst JR, van de Velde CJ, Frangioni JV. Image-guided cancer surgery using near-infrared fluorescence. Nat Rev Clin Oncol 2013;10:507–18. [PubMed: 23881033]

[64]. Themelis G, Yoo JS, Soh KS, Schulz R, Ntziachristos V. Real-time intraoperative fluorescence imaging system using light-absorption correction. J Biomed Opt 2009;14:064012. [PubMed: 20059250]

[65]. Matsui A, Lee BT, Winer J, Laurence RG, Frangioni JV. Quantitative assessment of perfusion and vascular compromise in perforator flaps using a near-infrared fluorescence guided imaging system. Plast Reconstr Surg 2009;124:451–60. [PubMed: 19644259]

[66]. Matsui A, Winer JH, Laurence RG, Frangioni JV. Predicting the survival of experimental ischaemic small bowel using intra-operative near-infrared fluorescence angiography. Br J Surg 2011;98:1725–34. [PubMed: 21953541]

[67]. Hoffman EJ, Tornai MP, Levin CS, MacDonald LR, Siegel S. Gamma and beta intra-operative imaging probes. Nucl Instrum Methods Phys Res A 1997;392:324–9.

[68]. Sironi S, Buda A, Picchio M, et al. Lymph node metastasis in patients with clinical early-stage cervical cancer: detection with integrated FDG PET/CT. Radiology 2006;238:272–9. [PubMed: 16304090]

[69]. Valdés RO, Vidal-Sicart S, Manca G, et al. Advances in radioguided surgery in oncology. Q J Nucl Med Mol Imaging 2017;61:247–70. [PubMed: 28569457]

[70]. Lyman GH, Giuliano AE, Somerfield MR, et al. American Society of Clinical Oncology guideline recommendations for sentinel lymph node biopsy in early-stage breast cancer. J Clin Oncol 2005;23:7703–20. [PubMed: 16157938]

[71]. Lees JE, Bugby SL, Bark A, Bassford DJ, Blackshaw P, Perkins A. A hybrid camera for locating sources of gamma radiation in the environment. J Instrum 2013;8:P10021.

[72]. Keshtgar M, Ell P. Sentinel lymph node detection and imaging. Eur Nucl Med 1999;26:57–67.

[73]. Heller S, Zanzonico P. Nuclear probes and intraoperative gamma cameras. Semin Nucl Med 2011;41:166–81. [PubMed: 21440694]

[74]. Fusco JC, Seynnaeve BK, Davit AJ III, et al. Use of intraoperative nuclear imaging leads to decreased anesthesia time and real-time confirmation of lesion removal. J Pediatr Surg 2018;53:77–80.

[75]. Ozkan E, Eroglu A. The utility of intraoperative handheld gamma camera for detection of sentinel lymph nodes in melanoma. Nucl Med Mol Imaging 2015;49:318–20. [PubMed: 26550052]

[76]. Kaviani S, Zeraatkar N, Sajedi S, et al. Design and development of a dedicated portable gamma camera system for intra-operative imaging. Phys Med 2016;32:889–97. [PubMed: 27345258]

[77]. Mathelin C, Salvador S, Huss D, Guyonnet J-L. Precise localization of sentinel lymph nodes and estimation of their depth using a prototype intraoperative mini-camera in patients with breast cancer. J Nucl Med 2007;48:623–9. [PubMed: 17401101]

[78]. Salvador S, Bekaert V, Mathelin C, Guyonnet J, Huss D. An operative gamma camera for sentinel lymph node procedure in case of breast cancer. J Instrum 2007;2:P07003.

[79]. Paredes P, Vidal-Sicart S, Zanón G, et al. Radioguided occult lesion localisation in breast cancer using an intraoperative portable gamma camera: first results. Eur J Nucl Med Mol Imaging 2008;35:230–5. [PubMed: 18043918]

[80]. Vermeeren L, Olmos RAV, Klop WMC, Balm AJ, van den Brekel MW. A portable [gamma]-camera for intraoperative detection of sentinel nodes in the head and neck region. J Nucl Med 2010;51:700–3. [PubMed: 20395319]

[81]. Tanaka C, Fujii H, Shiotani A, Kitagawa Y, Nakamura K, Kubo A. Sentinel node imaging of laryngeal cancer using a portable gamma camera with CdTe semiconductor detectors. Clin Nucl Med 2005;30:440–3. [PubMed: 15891306]

[82]. Tsuchimochi M, Hayama K, Oda T, Togashi M, Sakahara H. Evaluation of the efficacy of a small CdTe □-camera for sentinel lymph node biopsy. J Nucl Med 2008;49:956–62. [PubMed: 18483107]

[83]. Fujii H, Kitagawa Y, Kitajima M, Kubo A. Sentinel nodes of malignancies originating in the alimentary tract. Ann Nucl Med 2004;18:1–12. [PubMed: 15072178]

[84]. Brouwer OR, Valdés Olmos R, Vermeeren L, Hoefnagel CA, Nieweg OE, Horenblas S. SPECT/CT and a portable c-camera for image-guided laparoscopic sentinel node biopsy in testicular cancer. J Nucl Med 2011;52:551–4. [PubMed: 21421720]

[85]. Vermeeren L, Valdes Olmos RA, Meinhardt W, et al. Intra-operative radioguidance with a portable gamma camera: a novel technique for laparoscopic sentinel node localisation in urological malignancies. Eur J Nucl Med Mol Imaging 2009;36:1029–36. [PubMed: 19288098]

[86]. Betancourt Hernandez JA, Vera Donoso C, Martinez-Sarmiento M, Monserrat JJ, Bello Jarque P, Boronat Tormo F. Application of the radio-guided occult lesion localization technique for renal lumpectomy: from the laboratory to the patient. Clin Nucl Med 2017;42:e467–e8. [PubMed: 28825950]

[87]. Geurts N, Lamb AD, Lawrentschuk N, Murphy DG. Prostate-specific membrane antigen radioguided surgery: a promising utility. BJU Int 2017;120:5–6.

[88]. Kitagawa W, Shimizu K, Akasu H. Radioguided parathyroidectomy for primary hyperparathyroidism using the solid-state, multi-crystal gamma camera. Med Sci Monit 2003;9:CS53–CS6. [PubMed: 12824955]

[89]. Ortega J, Ferrer-Rebolleda J, Cassinello N, Lledo S. Potential role of a new hand-held miniature gamma camera in performing minimally invasive parathyroidectomy. Eur J Nucl Med Mol Imaging 2007;34:165–9. [PubMed: 17033847]

[90]. Vidal i Sicart S, Paredes P, Zanón G, et al. Added value of intra-operative real-time imaging in searches for difficult-to-locate sentinel nodes. J Nucl Med 2010;51:1219–25. [PubMed: 20660385]

[91]. Newman LA. Current issues in the surgical management of breast cancer: a review of abstracts from the 2002 San Antonio Breast Cancer Symposium, the 2003 Society of Surgical Oncology annual meeting, and the 2003 American Society of Clinical Oncology meeting. Breast J 2004;10:S22–S5. [PubMed: 14984486]

[92]. Tsuchimochi M, Hayama K. Intraoperative gamma cameras for radioguided surgery: technical characteristics, performance parameters, and clinical applications. Phys Med 2013;29:126–38. [PubMed: 22672926]

[93]. Hellingman D, Vidal-Sicart S, Paredes P, Olmos RAV. A new portable hybrid camera for fused optical and scintigraphic imaging: first clinical experiences. Clin Nucl Med 2016;41:e39–e43. [PubMed: 26053725]

[94]. Goyal A, Newcombe RG, Mansel RE. Role of routine preoperative lymphoscintigraphy in sentinel node biopsy for breast cancer. Eur J Cancer 2005;41:238–43. [PubMed: 15661548]

[95]. Knoll P, Mirzaei S, Schwenkenbecher K, Barthel T. Performance evaluation of a solid-state detector based handheld gamma camera system. Front Biomed Technol 2014;1:61–7.

[96]. Bugby SL, Lees JE, Bhatia BS, Perkins AC. Characterisation of a high resolution small field of view portable gamma camera. Phys Med 2014;30:331–9. [PubMed: 24225012]

[97]. Siman W, Cheenu Kappadath S. Performance characteristics of a new pixelated portable gamma camera. Med Phys 2012;39(6Part1):3435–44. [PubMed: 22755723]

[98]. Abe A, Takahashi N, Lee J, et al. Performance evaluation of a hand-held, semiconductor (CdZnTe)-based gamma camera. Eur J Nucl Med Mol Imaging 2003;30:805–11. [PubMed: 12677308]

[99]. Russo P, Curion AS, Mettivier G, et al. Evaluation of a CdTe semiconductor based compact gamma camera for sentinel lymph node imaging. Med Phys 2011;38:1547–60. [PubMed: 21520866]

[100]. Pitre S, Ménard L, Ricard M, Solal M, Garbay J-R, Charon Y. A hand-held imaging probe for radio-guided surgery: physical performance and preliminary clinical experience. Eur J Nucl Med Mol Imaging 2003;30:339–43. [PubMed: 12634960]

[101]. Sanchez F, Fernandez M, Gimenez M, et al. Performance tests of two portable mini gamma cameras for medical applications. Med Phys 2006;33:4210–20. [PubMed: 17153400]

[102]. Tsuchimochi M, Sakahara H, Hayama K, et al. A prototype small CdTe gamma camera for radioguided surgery and other imaging applications. Eur J Nucl Med Mol Imaging 2003;30:1605–14. [PubMed: 14504828]

[103]. Aarsvod JN, Greene CM, Mintzer RA, et al. Intraoperative gamma imaging of axillary sentinel lymph nodes in breast cancer patients. Phys Med 2006;21:76–9. [PubMed: 17646000]

[104]. Hruska CB, O'Connor MK. CZT detectors: How important is energy resolution for nuclear breast imaging? Phys Med 2006;21:72–5. [PubMed: 17645999]

[105]. Massari R, Ucci A, Campisi C, Scopinaro F, Soluri A. A novel fully integrated handheld gamma camera. Nucl Instrum Methods Phys Res A 2016;832:271–8.

[106]. Del Guerra A, Belcari N, Bisogni MG, et al. Advantages and pitfalls of the silicon photomultiplier (SiPM) as photodetector for the next generation of PET scanners. Nucl Instrum Methods Phys Res A 2010;617:223–6.

[107]. Haneishi H, Shimura H, Hayashi H. Image synthesis using a mini gamma camera and stereo optical cameras. IEEE Trans Nucl Sci 2010;57:1132–8.

[108]. Piert M, Burian M, Meisetschläger G, et al. Positron detection for the intraoperative localisation of cancer deposits. Eur J Nucl Med Mol Imaging 2007;34:1534–44. [PubMed: 17431612]

[109]. Spadola S, Verdier M-A, Pinot L, et al. Design optimization and performances of an intraoperative positron imaging probe for radioguided cancer surgery. J Instrum 2016;11:P12019.

[110]. Tipnis S, Nagarkar V, Shestakova I, et al. Feasibility of a beta-gamma digital imaging probe for radioguided surgery. IEEE Trans Nucl Sci 2004;51:110–6.

[111]. Sabet H, Stack BC, Nagarkar VV. A hand-held, intra-operative positron imaging probe for surgical applications. IEEE Trans Nucl Sci 2015;62:1927–34.

[112]. Monge F, Shakir DI, Lejeune F, Morandi X, Navab N, Jannin P. Acquisition models in intraoperative positron surface imaging. Int J Comput Assist Radiol Surg 2017;12:691–703. [PubMed: 27714566]

[113]. Andersen P, Chakera A, Klausen T, et al. Radiation exposure to surgical staff during F-18-FDG-guided cancer surgery. Eur J Nucl Med Mol Imaging 2008;35:624–9. [PubMed: 17955240]

[114]. Cremonesi M, Ferrari M, Sacco E, Rossi A, De Cicco C. Radiation protection in radioguided surgery of breast cancer. Nucl Med Commun 1999;20:919–24. [PubMed: 10528297]

[115]. Klausen T, Chakera A, Friis E, Rank F, Hesse B, Holm S. Radiation doses to staff involved in sentinel node operations for breast cancer. Clin Physiol Funct Imaging 2005;25:196–202. [PubMed: 15972020]

[116]. Povoski SP, Sarikaya I, White WC, et al. Comprehensive evaluation of occupational radiation exposure to intraoperative and perioperative personnel from 18 F-FDG radioguided surgical procedures. Eur J Nucl Med Mol Imaging 2008;35:2026–34. [PubMed: 18618106]

[117]. Cousins C, Miller D, Bernardi G, et al. International commission on radiological protection. ICRP publication 2011;120:1–125.

[118]. Wendler T, Herrmann K, Schnelzer A, et al. First demonstration of 3-D lymphatic mapping in breast cancer using freehand SPECT. Eur J Nucl Med Mol Imaging 2010;37:1452–61. [PubMed: 20354851]

[119]. Mihaljevic AL, Rieger A, Belloni B, et al. Transferring innovative freehand SPECT to the operating room: first experiences with sentinel lymph node biopsy in malignant melanoma. Eur J Surg Oncol 2014;40:42–8. [PubMed: 24084086]

[120]. Bluemel C, Herrmann K, Kubler A, et al. Intraoperative 3-D imaging improves sentinel lymph node biopsy in oral cancer. Eur J Nucl Med Mol Imaging 2014;41:2257–64. [PubMed: 25077931]

[121]. Jeschke S, Lusuardi L, Myatt A, Hruby S, Pirich C, Janetschek G. Visualisation of the lymph node pathway in real time by laparoscopic radioisotope-and fluorescence-guided sentinel lymph node dissection in prostate cancer staging. Urology 2012;80:1080–7. [PubMed: 22990053]

[122]. Brouwer OR, van den Berg NS, Mathéron HM, et al. A hybrid radioactive and fluorescent tracer for sentinel node biopsy in penile carcinoma as a potential replacement for blue dye. Eur Urol 2014;65:600–9. [PubMed: 24355132]

[123]. KleinJan GH, Hellingman D, van den Berg NS, et al. Hybrid surgical guidance: does hardware integration of gamma-and fluorescence-imaging modalities make sense. J Nucl Med 2017;58:646–50. [PubMed: 27688478]

[124]. van den Berg NS, Simon H, Kleinjan GH, et al. First-in-human evaluation of a hybrid modality that allows combined radio- and (near-infrared) fluorescence tracing during surgery. Eur J Nucl Med Mol Imaging 2015;42:1639–47. [PubMed: 26109329]

[125]. Kang HG, Lee HY, Kim KM, Song SH, Hong GC, Hong SJ. A feasibility study of an integrated NIR/gamma/visible imaging system for endoscopic sentinel lymph node mapping. Med Phys 2017;44:227–39. [PubMed: 28102947]

[126]. KleinJan GH, van den Berg NS, van Oosterom MN, et al. Towards (hybrid) navigation of a fluorescence camera in an open surgery setting. J Nucl Med 2016;57:1650–3. [PubMed: 27230927]

[127]. Emerson DK, Limmer KK, Hall DJ, et al. A receptor-targeted fluorescent radiopharmaceutical for multireporter sentinel lymph node imaging. Radiology 2012;265:186–93. [PubMed: 22753678]

[128]. Hosseini A, Baker JL, Tokin CA, et al. Fluorescent-tilmanocept for tumor margin analysis in the mouse model. J Surg Res 2014;190:528–34. [PubMed: 24923630]

[129]. Hekman MC, Rijpkema M, Muselaers CH, et al. Tumor-targeted dual-modality imaging to improve intraoperative visualization of clear cell renal cell carcinoma: a first in man study. Theranostics 2018;8:2161–70. [PubMed: 29721070]

[130]. Li Z, Zhang G, Shen H, Zhang L, Wang Y. Synthesis and cell uptake of a novel dualmodality 188Re-HGRGD (D) F-CdTe QDs probe. Talanta 2011;85:936–42. [PubMed: 21726721]

[131]. Duheron V, Moreau M, Collin B, et al. Dual labeling of lipopolysaccharides for SPECT-CT imaging and fluorescence microscopy. ACS Chem Biol 2013;9:656–62. [PubMed: 24328371]

[132]. Wang Y, An F-F, Chan M, et al. 18F-positron-emitting/fluorescent labeled erythrocytes allow imaging of internal hemorrhage in a murine intracranial hemorrhage model. J Cereb Blood Flow Metab 2017;37:776–86. [PubMed: 28054494]

[133]. An F-F, Kommidi H, Chen N, Ting R. A conjugate of pentamethine cyanine and 18F as a positron emission tomography/near-infrared fluorescence probe for multimodality tumor imaging. Int J Mol Sci 2017;18:1214.

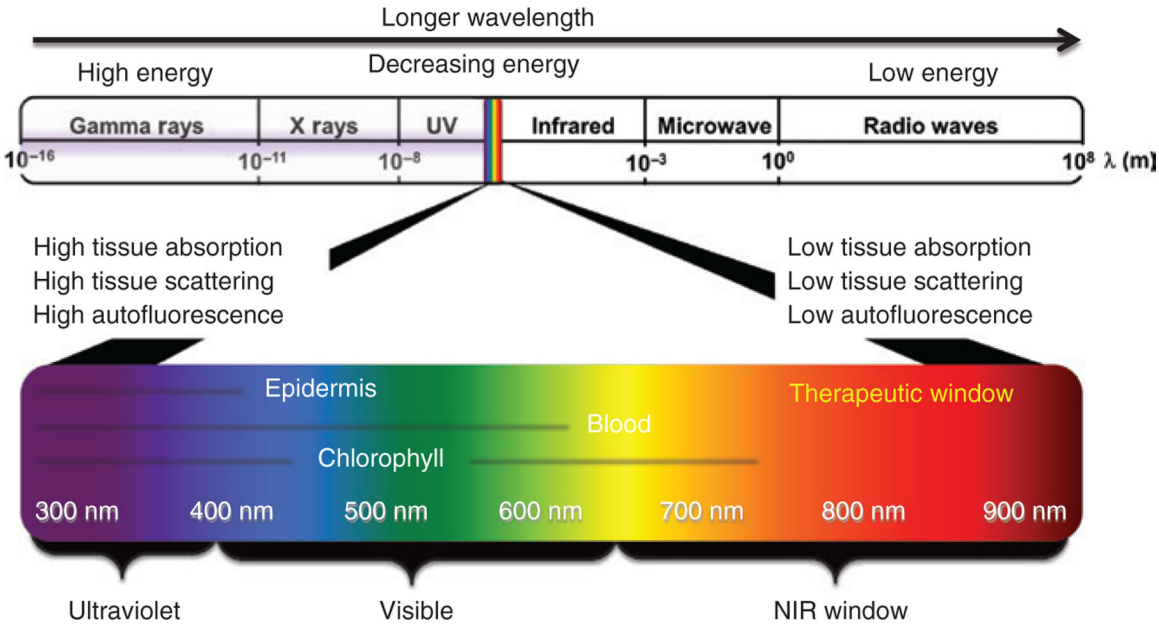

Figure 1. Electromagnetic radiation spectrum from gamma rays to radio waves.

The fluorescence wavelength includes UV (200–400 nm), visible radiation (400–650 nm), and NIR (650–900 nm). The NIR window is considered as the therapeutic window due to the low tissue absorption, low tissue scattering, and low autofluorescence. Reproduced with permission from [2].

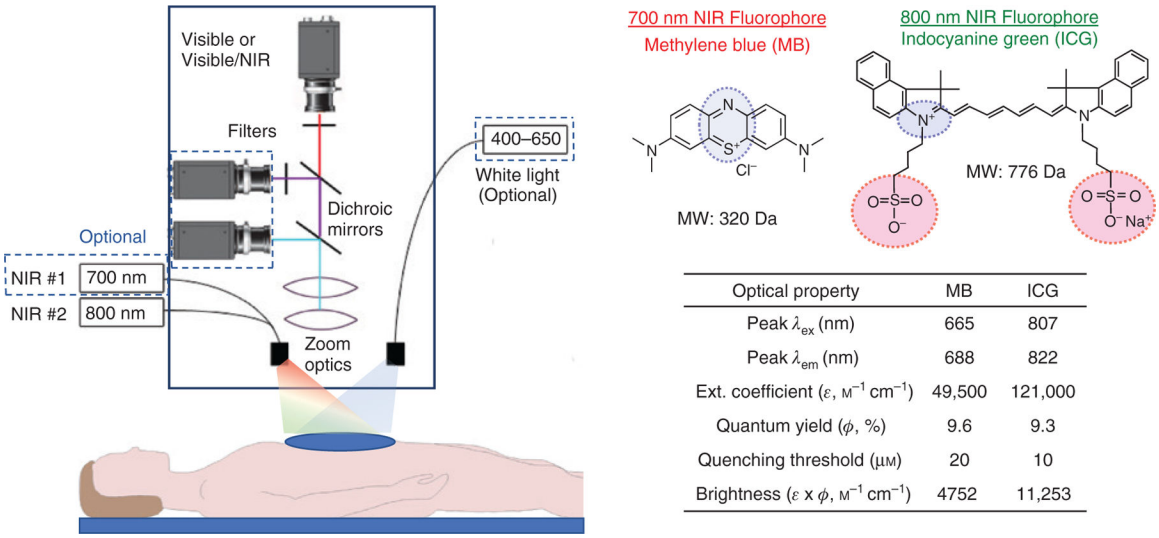

Optical property	MB	ICG
Peak λ_{ex} (nm)	665	807
Peak λ_{em} (nm)	688	822
Ext. coefficient (ε, M^{-1} cm^{-1})	49,500	121,000
Quantum yield (ϕ, %)	9.6	9.3
Quenching threshold (μM)	20	10
Brightness (ε x ϕ, M^{-1} cm^{-1})	4752	11,253

Figure 2. Real-time image-guided surgery using a multichannel NIR imaging system combined with currently available NIR fluorophores in clinical use.

MB is used for the 700 nm emitting NIR channel, and ICG is for the 800 nm NIR channel. Blue dotted squares indicate optional components. Reproduced with permission from [11].

Figure 3. Commercially available open-air NIR fluorescence imaging systems for image-guided surgery.

Shown are representative images of SPY Elite (Novadaq), PDE (Hamamatsu), SPY PHI (Novadaq), Fluobeam (Fluoptics), Spectrum (Quest Medical Imaging), VisionSense (Iridium), and Vitom II ICG (Karl Storz). Reproduced with permission from [13, 15].

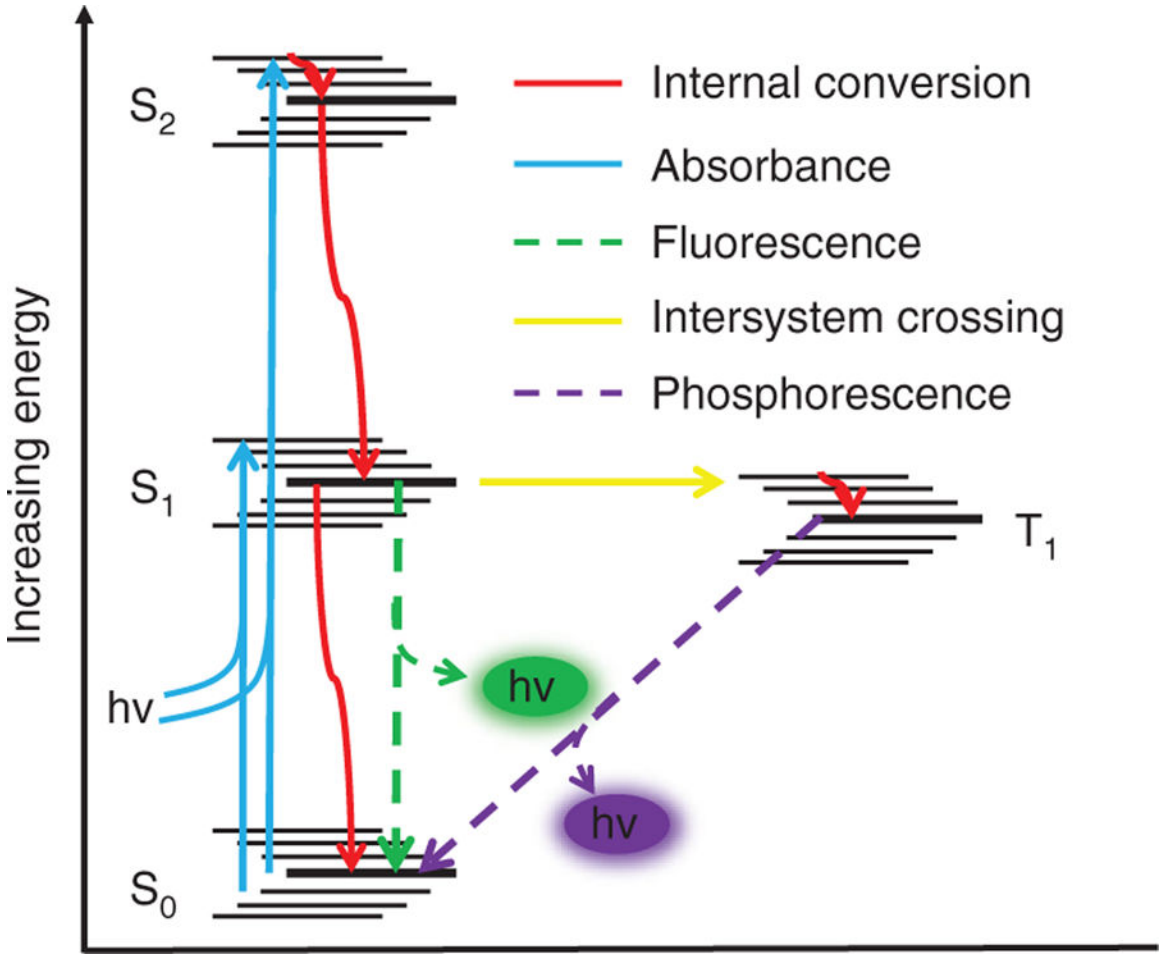

Figure 4. Jablonski diagram showing fluorescence and competing pathways for molecular relaxation from an excited state.

Reproduced with permission from [10].

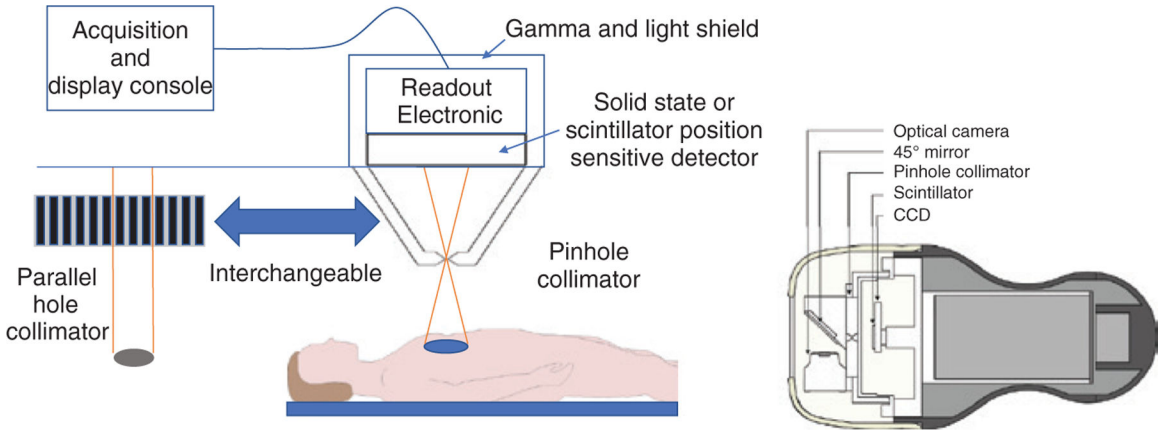

Figure 5. Intraoperative gamma imaging using a pinhole collimator.

A mirror at the entrance of pin-hole collimator is used to reflect optical photons to the CCD camera and produce coregistered images of optical and gamma photons. Reproduced with permission from [71].

Figure 6. Portable and handheld commercial gamma cameras for intraoperative use.
Reproduced with permission from [73–76].

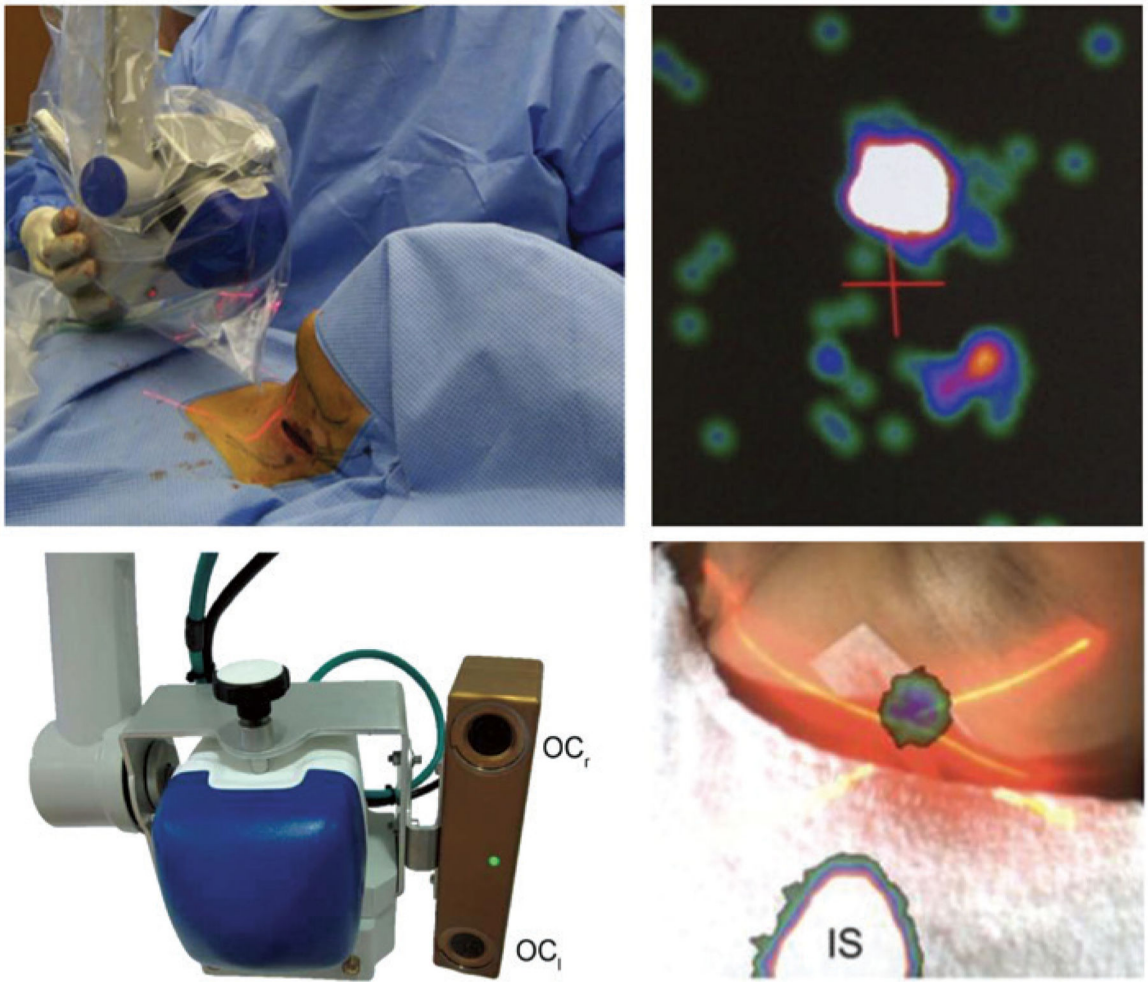

Figure 7. Optical images help surgeons to better localize SLNs in patients.

The laser pointer can work as a reference to localize the center of FOV in the image and patient (top). Reproduced with permission from [92]. Optical cameras mounted beside commercial systems can be used to overlay both images on display using image processing methods (bottom). Reproduced with permission from [34, 93].

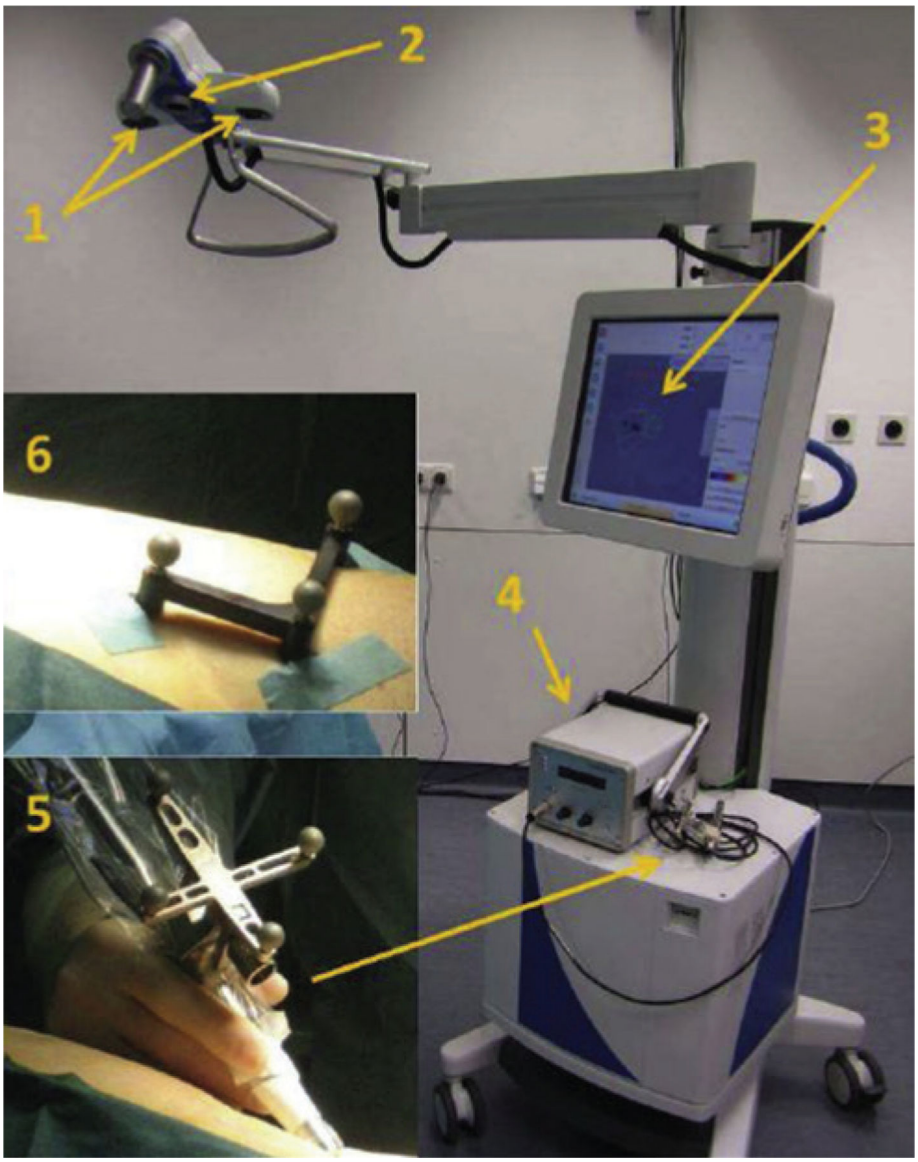

Figure 8. Surgical setup of a freehand SPECT system by Declipse (Surgieye, Munich, Germany). The freehand 3D SPECT is composed of two calibrated infrared cameras (1) to determine accurate position of gamma probe in respect to the patient body using two tracking objects on patient (6) and gamma probe (5); and an optical camera (2) to record procedure flow and fuse the gamma distribution image to optical view of operation area in the display screen (3). A conventional gamma probe (4) generates gamma distribution data for 3D image creation before and after resection, as well as produces acoustic and visual feedback of gamma distribution during surgical procedures. Reprinted with permission from [119].

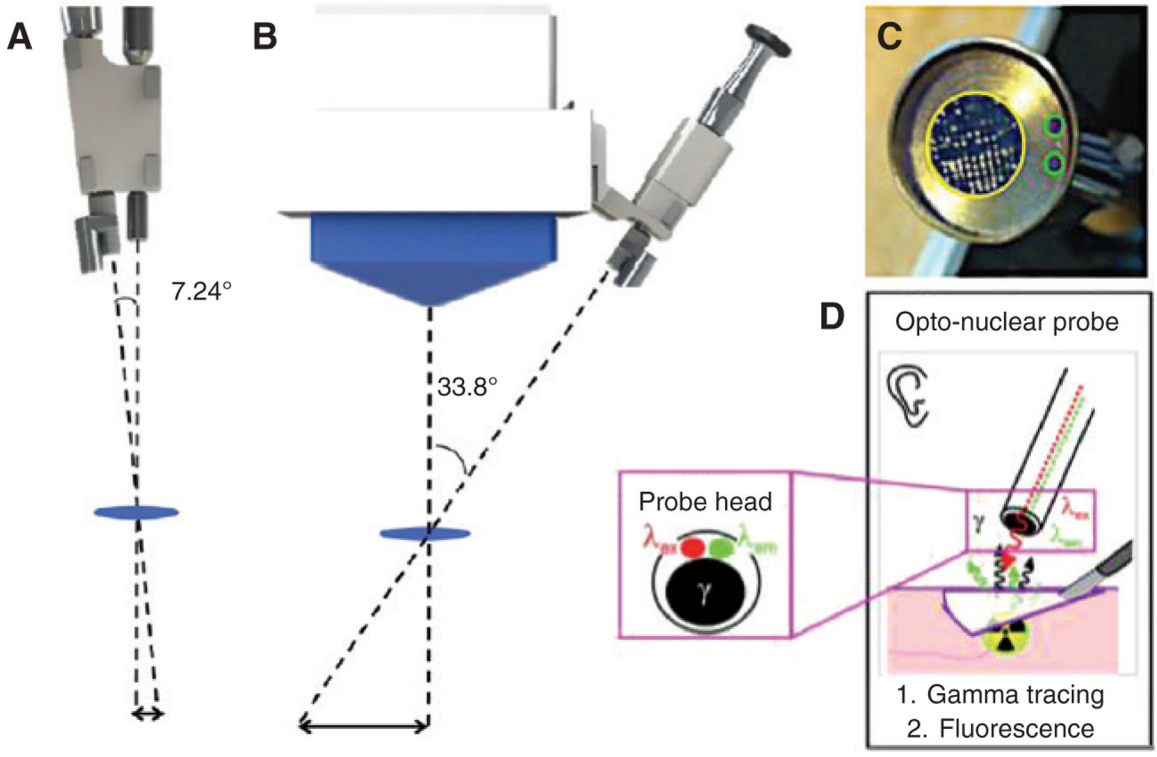

Figure 9. Dual modal imaging devices composed of a gamma probe/camera and a fluorescence camera to image fluorescence and gamma tracers.

(A) Aligned type combination of gamma probe and fluorescence camera and (B) flexible type combination of gamma and fluorescence cameras to compensate the misalignment at distances beyond the focal plane. Reproduced with permission from [123]. (C) A prototype gamma probe in conjunction with two fiber optics to excite and collect emission photons and (D) conceptual drawing of the opto-nuclear probe shown in (C). Reproduced with permission from [124].

Table 1:

Commercially available open-air imaging systems for image-guided surgery [12, 14, 54].

Device	Company	Mode	Excitation source	# of channels	Image overlay	Excitation (nm)	FOV (cm^2)	WD (cm)	Sensitivity	FDA approval
SPY Elite	Novadaq	Open-air	LD	2	Yes	805	19 × 14	~30	5	2005
FL800	Leica	Surgical microscope	Xenon	2	Yes	700−800	NA	NA	NA	2006
Infrared 800	Zeiss	Surgical microscope	Xenon	2	Yes	700−780	NA	20–63	NA	2010
PDE	Hamamatsu	Handheld	LED	1	No	760	5 × 5−10 × 6.7	~20	15	2012
Firefly for Da Vinci	Novadaq/Intuitive	Robotic	LD	2	No	805−830	NA	NA	NA	2014
Fluobeam	Fluoptics	Handheld	LD	1	No	680 or 750	2.2 × 1.5−20 × 14	25−50	5	2014
Artemis (Spectrum)	Quest Medical	Open-air	LED	3	Yes	400−1000	2.2 × 2.2	~5	10	2015
Vision-Sense	Iridium	Open-air	LD	2	Yes	805	19 × 14	~30	0.05	2015
Vitom ICG	Karl Storz	Open-air laparoscopy	Xenon	2	No	NA	NA	20−30	NA	2016
Pinpoint	Novadaq	Endoscopy	LD	2	Yes	805	NA	32	NA	2016
SPY PHI	Novadaq	Handheld	LD	2	No	806	7.6 × 5.0 19 × 13	30	NA	2017

FOV, Field-of-view; WD, working distance; NA, not available.

Table 2:

Clinically reported intraoperative gamma cameras.

Device	Company	Usage	Detector type	Detector size (cm^2)	Energy res. (%)	Intrinsic spatial res. (mm)	System spatial res. (mm)	Collimator	FDA approval
CrystalCAM [95]	Crystal Photonics	Handheld	CZT	4 × 4	7	2.46	5.0 (@5 cm LEHR)	Parallel hole	NA
CGC [96]	Lab use	Handheld	CsI(Tl)/EMCCD	0.8 × 0.8	58	0.63	1.3 (@1.3 cm)	Pinhole	NA
ERGO [97]	Digirad	Portable	CsI(Tl)/Photodiode	40 × 31	7.4	3.3	4.9 (5 cm, LEHR)	Parallel hole	2010
eZ-Scope [98]	Lab use	Handheld	CZT	32 × 32	8.6	1.85	7.8 (@5 cm, LEHR)	Parallel hole	2002
MediPROBE [99]	Lab use	Handheld	CdTe	1.4 × 1.4	–	0.055	5.6 (@5 cm)	Pinhole	NA
POCI [100]	Lab use	Handheld	CsI(Na)/Photodiode	4 (diameter)	32	2.3	7.6 (@5 cm)	Parallel hole	NA
Sentinella [101]	Oncovision	Handheld	CsI(Na)/PS-PMT	4 × 4	15.9	1.8	6.1 (@5 cm)	Parallel/ pinhole	2009
Sergeosight [76]	PNP	Handheld	Cs(Tl)/PS-PMT	5 × 5	21	2.2	8.0 (@5 cm)	Parallel/ pinhole	NA
SSGC [82, 102]	Lab use	Handheld	CdTe	4.5 × 4.5	6.9	1.59	7.2 (@5 cm)	Parallel hole	NA

CZT, Cadmium zinc telluride; LEHR, low-energy high-resolution; PS-PMT, position sensitive photomultiplier tube; NA, not approved.

Table 3:

Radiation dose associated with ^{18}F and ^{99m}Tc isotopes during image-guided surgeries.

Radioisotope	Injected dose (MBq)	Absorbed dose: patient (mGy)	Effective dose: surgeon (μSv)	Effective dose: nurse (μSv)	Annual dose limit (mSv/y)
^{99m}Tc [114]	11	10.3	0.9	0.7	20
^{99m}Tc[a] [115]	88	NA	40	NA	20
^{18}F-FDG [113]	45	NA	16/h	NA	20
^{18}F-FDG[a] [116]	699	NA	164/h	83/h	20

[a]With preoperative nuclear imaging. FDG, Fluorodeoxyglucose; NA, not available.